

PAPER • OPEN ACCESS

Upper stimulation threshold for retinal ganglion cell activation

To cite this article: Kevin Meng *et al* 2018 *J. Neural Eng.* **15** 046012

View the [article online](#) for updates and enhancements.

Related content

- [Retinal ganglion cells: mechanisms underlying depolarization block and differential responses to high frequency electrical stimulation of ON and OFF cells](#)
T Kameneva, M I Maturana, A E Hadjinicolaou *et al.*
- [The impact of calcium current reversal on neurotransmitter release in the electrically stimulated retina](#)
Paul Werginz and Frank Rattay
- [Differential electrical responses in retinal ganglion cell subtypes: effects of synaptic blockade and stimulating electrode location](#)
Chih Yu Yang, David Tsai, Tianruo Guo *et al.*

Recent citations

- [In vitro assessment of the differences in retinal ganglion cell responses to intra- and extracellular electrical stimulation](#)
Rebecca Kotsakidis *et al*



IOP | ebooks™

Bringing you innovative digital publishing with leading voices to create your essential collection of books in STEM research.

Start exploring the collection - download the first chapter of every title for free.

Upper stimulation threshold for retinal ganglion cell activation

Kevin Meng^{1,2,7}, Andreas Fellner^{3,7} , Frank Rattay³ , Diego Ghezzi⁴ ,
Hamish Meffin^{1,5} , Michael R Ibbotson^{1,5}  and Tatiana Kameneva^{2,6} 

¹ National Vision Research Institute, Australian College of Optometry, Australia

² Department of Biomedical Engineering, The University of Melbourne, Australia

³ Institute for Analysis and Scientific Computing, Vienna University of Technology, Vienna, Austria

⁴ Medtronic Chair in Neuroengineering, Ecole Polytechnique Federale de Lausanne (EPFL),

Lausanne, Switzerland

⁵ Department of Optometry and Vision Sciences, University of Melbourne, Australia

⁶ Faculty of Science, Engineering and Technology, Swinburne University of Technology, Australia

E-mail: tkameneva@swin.edu.au (Tatiana Kameneva)

Received 24 October 2017, revised 15 February 2018

Accepted for publication 4 April 2018

Published 9 May 2018



Abstract

Objective. The existence of an upper threshold in electrically stimulated retinal ganglion cells (RGCs) is of interest because of its relevance to the development of visual prosthetic devices, which are designed to restore partial sight to blind patients. The upper threshold is defined as the stimulation level above which no action potentials (direct spikes) can be elicited in electrically stimulated retina. **Approach.** We collected and analyzed *in vitro* recordings from rat RGCs in response to extracellular biphasic (anodic-cathodic) pulse stimulation of varying amplitudes and pulse durations. Such responses were also simulated using a multicompartiment model. **Main results.** We identified the individual cell variability in response to stimulation and the phenomenon known as upper threshold in all but one of the recorded cells ($n = 20/21$). We found that the latencies of spike responses relative to stimulus amplitude had a characteristic U-shape. *In silico*, we showed that the upper threshold phenomenon was observed only in the soma. For all tested biphasic pulse durations, electrode positions, and pulse amplitudes above lower threshold, a propagating action potential was observed in the distal axon. For amplitudes above the somatic upper threshold, the axonal action potential back-propagated in the direction of the soma, but the soma's low level of hyperpolarization prevented action potential generation in the soma itself. **Significance.** An upper threshold observed in the soma does not prevent spike conductance in the axon.

Keywords: retinal ganglion cells, electrical stimulation, visual prosthesis, stimulation threshold

(Some figures may appear in colour only in the online journal)

1. Introduction

Pathologies of the visual system are diverse in their causes and can affect any level of the visual pathway. Age-related macular degeneration (AMD) and retinitis pigmentosa (RP) are medical conditions that lead to the atrophy of photoreceptors, the light-sensitive cells in the retina that convert light

energy into electrochemical signals, which are then transmitted through complex neural retinal networks to the visual cortex. AMD is the leading cause of visual impairment in elderly people. The estimated number of people with AMD in 2020 is 196 million (Wong *et al* 2014). The prevalence of RP is approximately 1 in 4000 (Hamel 2006). The early stages of AMD may include a change in the quality of vision with the straight lines appearing distorted and some visual areas appearing blurry. The later stages of AMD cause blindness.

⁷ Equal first authors.



The first sign of RP is usually a loss of night vision, with increased occurrence of blind spots that gradually lead to the loss of vision in later stages.

In patients with AMD and RP, it is possible to create visual perception through electrical stimulation. Electrical stimulation of remaining neurons in the retina with retinal prostheses is the most developed field of research (Weiland and Humayun 2014, Hadjinicolaou *et al* 2015). To improve efficacy of retinal prostheses, multiple studies have characterized individual retinal ganglion cells (RGCs) in terms of their electrophysiological responses to different patterns of electrical stimulation (Jensen and Rizzo 2007, Freeman *et al* 2011, Tsai *et al* 2012, Maturana *et al* 2016).

Different types of prosthetic systems have been developed (Yue *et al* 2016). They differ in their location on the retina and their components. The implant can be placed epiretinally (on the ganglion cell side of the retina), subretinally (on the photoreceptor side), or suprachoroidally (between the choroid and sclera).

Electrical stimulation consists of a series of biphasic current pulses, which can be either cathodic-first or anodic-first. In addition, to achieve safe stimulation for the survival of both the tissue and the electrodes, each pulse is generally charge-balanced, so the net charge injected is zero. The choice of polarity may have implications at the perceptual level but there is currently no psychophysical study that examines this in detail.

Given a fixed pulse duration, the increase in activation probability can be approximated using a sigmoidal curve (Tsai *et al* 2009). The pulse amplitude associated with 50% activation is usually defined as the threshold of activation. It is often assumed that the activation curve of individual RGCs reaches saturation above a certain amount of injected charge. However, a recent study has reported a drop of the activation curve, known as the ‘upper threshold phenomenon’, which occurs before the threshold of cellular damage (Boinagrov *et al* 2012). The stimulation amplitude above which there are no action potentials (no direct spikes elicited at stimulation), is defined as upper threshold (see figure 1(A)). The decrease in activation probability takes the shape of a negative sigmoid, as illustrated in figure 1. Similar decreases in the number of spikes (negative sigmoid shaped activation function at very high amplitudes of stimulation) were observed *in vitro* by Barriga-Rivera *et al* (2017). In two papers (Boinagrov *et al* 2012, Barriga-Rivera *et al* 2017), monophasic pulse stimulation was used *in vitro*. However, for the safety reasons outlined above, biphasic pulses are now used in the clinic.

The mechanisms behind the upper threshold phenomenon are still unclear. Using computer simulation of a spherical cell and a Hodgkin–Huxley type model, Boinagrov and colleagues (Boinagrov *et al* 2012) proposed a hypothesis that this phenomenon is caused because the sodium reversal potential is reached at high stimulation levels (i.e. approximately 35 mV, Fohlmeister and Miller (1997)), leading to a change in the direction of the sodium current so that it tends to counter the depolarization of the cell. However, Rattay (2014) has shown using a model in which the geometry of the cell is taken into account (i.e. soma plus axon), that the longitudinal component

of the electrical stimulation becomes dominant (Meffin *et al* 2012), leading to depolarization and spikes in the axon that cannot propagate to the soma due to strong hyperpolarization. Again, in both papers (Boinagrov *et al* 2012, Rattay 2014) simulations were conducted with monophasic pulses. It remains to be proven if the upper threshold at the soma would hold with biphasic stimulation.

Here, we investigated the upper threshold phenomenon *in vitro* using biphasic pulses of various amplitudes and phase durations. The upper threshold phenomenon was observed for direct spikes recorded in the soma in all but one of our cells. Similar to Boinagrov *et al* (2012), we observed a U-shaped pattern of stimulation latencies. This pattern was observed for stimulation with all phase durations except for 0.25 ms. Long latency spikes (occurring ≥ 4 ms after stimulation) did not show the upper threshold phenomenon up to the limit imposed by our stimulator.

To test the hypothesis of the mechanisms underlying the upper threshold phenomenon proposed for monophasic pulses (Boinagrov *et al* 2012), we simulated a modified multi-compartment model using the Hodgkin–Huxley type formalism (Fohlmeister and Miller 1997, Rattay 2014). The computer simulations are not meant to reproduce the experiments in detail, but they concentrate on the upper threshold phenomena, which seems not to depend essentially on the shape of the electrode. Instead, a strong extracellular potential gradient along the soma surface is crucial for the phenomenon, which is reflected by the spherical symmetry of the electric field generated by a point source. In contrast to a disc electrode, the point source simulates the tip of a micro-electrode.

Up to now, two different computer simulations have investigated the upper threshold phenomenon, both based on extracellular monophasic pulse stimulation. Boinagrov *et al* (2012) underlined their experimental findings with a model of a spherical soma consisting of 20 radial segments having a symmetric distribution of sodium ion channels around its surface. Further, to take effects of the highly excitable axon hillock of a RGC into account, also an asymmetric distribution of sodium ion channels among the spherical soma was considered and evaluated. In a reply to this study, Rattay (2014) presented a computer simulation of a dendrite-soma-axon RGC model where the soma consisted of three cylindrical compartments. Both soma and axon were investigated regarding action potentials at high stimulus amplitudes.

The model presented in this study, is the first computer simulation of a simplified RGC dealing with biphasic pulses in a highly spatially discretized multi-compartment model, which also considers the rotational symmetry of the electric field close to the tip of a stimulating microelectrode. We tested the simulated cell responses to different stimulation pulse configurations and stimulation electrode positions. Simulations showed that except for amplitudes very near the lower threshold, an action potential is always first initiated in the sodium band or axon hillock during the first (anodic) phase of biphasic pulse stimulation. The initiated action potential always propagated to the distal axon while back-propagation to the soma was blocked by the second (cathodic)

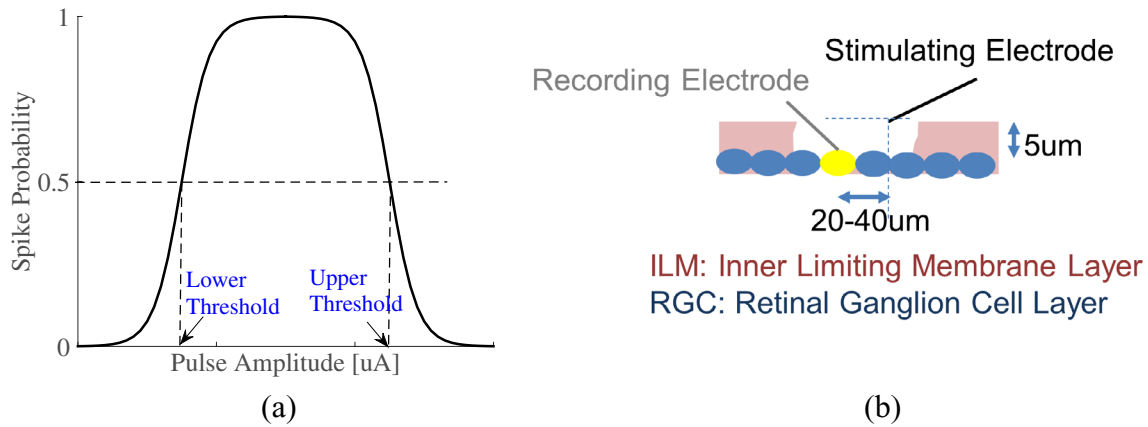


Figure 1. (A) A schematic diagram of RGC activation. (B) A cartoon of the experimental setup.

phase of the pulse in cases where a certain stimulus amplitude was exceeded.

2. Methods

2.1. Experiments

All protocols conformed to the policies of the National Health and Medical Research Council of Australia and were approved by the Animal Experimentation Ethics Committee of the University of Melbourne.

2.1.1. Retinal dissection. Data was collected from 15 female Long-Evans rats whose age was between two and six months. Each experimental session started with the extraction of retinal tissue, which was kept alive throughout the duration of the session. The animal was initially anesthetized with a mixture of Ketamine and Xylazine. Both optic cups were extracted and placed into an extracellular medium capable of supporting the retinal tissues (carbogenated Ames medium supplied with glucose and sodium bicarbonate). The animal was sacrificed immediately after the extraction by injection of 1 ml Lethabarb. Pieces of retina were mounted on a coverslip and held by a stainless steel harp placed in the centre of the perfusion chamber. Ganglion cells were facing up, such that they were accessible to patching pipettes. The retina was perfused at controlled room temperature with constant flow of extracellular medium at $3\text{--}8\text{ ml min}^{-1}$. The chamber was placed under a microscope equipped with a $20\times$ water immersion lens.

2.1.2. Patch-clamp recording. The inner limiting membrane was carefully scraped away with a sharp pipette to provide direct access to the underlying RGCs. The patching pipette was filled with $6.5\text{ }\mu\text{l}$ of an internal solution composed of K-glutamate (90%), energy cache (5%), biocytin (2.5%) and Alexa Hydrazide 488 (2.5%). Whole cell current-clamp recordings were obtained following standard procedures (Hamill *et al* 1981). Initial pipette resistance ranged between 5 and 15 $\text{M}\Omega$. A flow of internal solution was first applied through the pipette. The pipette voltage was then nulled in the bath, its resistance compensated with the bridge balance circuit of the amplifier, and its capacitance compensated. The

pipette was placed such that its tip slightly touched the membrane surface of the cell being patched. After a gigaseal was formed and the recorded potential stabilized close to resting potential, the membrane was ruptured by applying a brief but strong suction. The recorded voltage was amplified and digitally stored at an acquisition rate of 25 kHz. In all experiments, it was confirmed that the resting potential stabilized and remained constant throughout the whole experiment. Stimulation artifacts were blanked prior to spike detection. A blanking window depended on pulse duration. The values chosen for the blanking window were effective across all sessions. Blanking durations were 0.72, 0.88, 1.04, 1.20, 1.36, 1.52 ms for pulse phase durations 0.25, 0.375, 0.5, 0.625, 0.75, 0.875 ms, respectively.

2.1.3. Light and electrical stimulation. Retinas were dissected and kept in a low light condition before stimulation. Light stimulation was performed once, immediately after the successful patch. The mounted piece of retina was exposed to strong light for one second. The electrical behavior of the patched cell was analyzed at the onset and at the offset of the stimulus. The RGC classification into ON, OFF, or ON/OFF types, was done by observing the occurrence of spikes following the transition from dark to bright and from bright to dark. The cell was classified as an ON type, if its spike rate increased at light onset. The cell was classified as an OFF type if its spike rate increased at light offset. Cells that had an increase in spiking at both light onset and light offset were classified as ON-OFF types.

Electrical stimulation was performed using a Pt-Ir disk electrode with $100\text{ }\mu\text{m}$ diameter. The stimulation electrode was placed in the extracellular medium epiretinally prior to the patching process. The tip always faced the recording site. The distance to the recording site was kept constant across all cells and all experimental sessions; $20\text{--}40\text{ }\mu\text{m}$ to the side of the soma being patched and $5\text{ }\mu\text{m}$ above, touching the inner limiting membrane, as illustrated in figure 1(B). The return electrode was located at the other side of the chamber in the same bath.

A custom made Matlab interface (MathWorks, R2016a) was used to command a multi-channel stimulator (Tucker Davis Technologies IZ2-32 channels) and send different

waveform signals for stimulation. The amplitudes of stimulation were bounded by the limits of the stimulator at 300 μA .

The stimulation protocol consisted of repetitions of a train of randomized pulses of different phase durations and amplitudes. All pulses were biphasic, anodic-first, symmetric, and charge-balanced. The choice of anodic-first biphasic pulses in the experiments was based on the fact that it's easier to remove artifacts with anodic-first stimulation (i.e. see figure 3(B)—the action potentials are clearly distinguished from the artifacts). The computer simulation parameters followed the experimental protocol. No interphase gap was introduced. Phase duration varied from 0.25 to 0.875 ms, pulse amplitude varied from 0 to 300 μA . A pulse duration 0.25 ms refers to a 0.25 ms anodic (or cathodic) phase duration.

Cells were stimulated using a 20 Hz pulse train. The choice to use a low frequency of stimulation was made to avoid undesired dependency between consecutive pulses. The pulse train contained 366 pulses placed in random order. All combinations of pulse durations and pulse amplitudes were presented once (6 durations \times 61 amplitudes) per train. Pulse durations were selected between 0.25 and 0.875 ms with a step size of 0.25 ms. Pulse amplitudes were selected between 0 and 300 μA with a step size of 5 μA . The pulse train had a total duration of 18.3 s.

This pulse train was applied 16 times. This number of repetitions was large enough to provide an accurate estimate of the activation probability associated with each pulse, given pulse phase duration and amplitude. For each pulse duration, two generalized sigmoidal curves were fitted to the experimental data: one positive sigmoid for the growing part of the data and one negative sigmoid for the decreasing part. Spikes were classified into short-latency (within 4 ms of stimulus onset) and long-latency (≥ 4 ms) based on the time interval between stimulation artefact and detected spike. Fitting was performed using the least-squares approach. The dependent variable was pulse amplitude, while the independent variable was activation probability, defined here as the success rate of eliciting a spike after 16 repetitions for each amplitude.

$$y = \sigma(x) = \frac{1}{1 + \exp \frac{-(x-\beta_1)}{\beta_2}} \quad (1)$$

Equation (1) is the expression for the positive sigmoidal curve, with x being pulse amplitude, y being probability activation, and β_1 and β_2 the fitted parameters. Given a particular pulse duration, the activation threshold was defined as the pulse amplitude that elicits an action potential with a probability of 50%. The negative part of the sigmoid was obtained by substituting $-(x - \beta_1)$ with $x - \beta_1$ in (1). To fit the sigmoid curve to the data, the Matlab function *nlinfit* was used. It was assumed that sigmoidal curves start at zero and saturate at one.

2.2. Numerical simulation

Using NEURON 7.4 software (Hines 1993) in a Python 2.7 environment, a modified multi-compartment version of a simplified ganglion cell model (Rattay 2014) was stimulated from a point source to prove the existence of an upper threshold

for action potentials, as recorded in the soma. The segmentation axis of the soma was in the direction of the point source to take into account the rotational symmetry of the electric field during the stimulus (refer to figure 2). Figure 2 shows the geometry of the simplified RGC, consisting of a spherical soma ($d = 20 \mu\text{m}$, 21 truncated compartments with the axis in the direction of the electrode), a cylindrical axon hillock leaving the soma at the eastern pole with an inclination to North/East ending 2 μm above the soma ($l = 40 \mu\text{m}$, $d = 1 \mu\text{m}$, 40 cylindrical compartments in the xz direction), a conical sodium band ($l = 40 \mu\text{m}$, $d = 1-0.6 \mu\text{m}$, 40 truncated compartments in the x direction), a conical cylindrical thin segment ($l = 90 \mu\text{m}$, d between 0.6 and 1 μm , 90 truncated compartments in the x direction), and a cylindrical distal axon ($l = 200 \mu\text{m}$, $d = 1 \mu\text{m}$, 200 cylindrical compartments in the x direction). The cylindrical central dendrite is leaving the soma at the southern pole ($l = 10 \mu\text{m}$, $d = 4 \mu\text{m}$, 10 cylindrical compartments in the z direction) before diverging into a left and right cylindrical dendrite (each $l = 75 \mu\text{m}$, $d = 2 \mu\text{m}$, 75 cylindrical compartments in the x direction).

Note that changing from electrode position 1, e.g. to 3 or 5 (figure 2) caused another soma compartment to be connected with the axon hillock segment, whereas the central dendrite's connection to the soma compartment did not change for the investigated cases where $z_{\text{electrode}} = 15 \mu\text{m}$; the distance between the electrode and the z axis was 35 μm . The geometry was slightly modified from Jeng *et al* (2011) and Rattay (2014), and the diameters of axonal sections were in accordance with typical values as found in rat or cat retinas (Fohlmeister *et al* 2010). The axis of the sodium band and distal axonal segments were located 2 μm above the soma.

The (Fohlmeister and Miller 1997) model was used to simulate active cell behavior. The conductivities for sodium, g_{Na} , were based on Jeng *et al* (2011, table 1). The sodium band was assumed to have five times higher channel density than the soma leading to a g_{Na} of 400 ms cm^{-2} (Werginz *et al* 2014). Assuming constant ratios between single conductivities, all other conductivities (potassium, calcium, leakage) were determined based on the respective g_{Na} of each section and the ratios as given by Fohlmeister and Miller (1997). Intracellular resistivity was 0.3 $\text{k}\Omega \cdot \text{cm}$, and resistivity of the infinite extracellular medium, ρ_e , was 1 $\text{k}\Omega \cdot \text{cm}$. Temperature was set to 22 $^\circ\text{C}$ in simulations.

3. Results

3.1. Experiments

Out of the 21 cells used for our analyses, there were six ON type cells, eight OFF type cells, three ON-OFF type, and four cells with no light response (unknown class). Overall, no major difference regarding the RGC upper threshold phenomenon was detected across RGC classes. For all cells, only spikes with latencies below 10 ms were considered in the analysis.

Previous studies demonstrated that the activation probability curve of a single RGC follows a sigmoidal shape (Tsai *et al* 2009). This behavior was observed in all cells in our data set and is illustrated by the red curve in figure 3(A) for

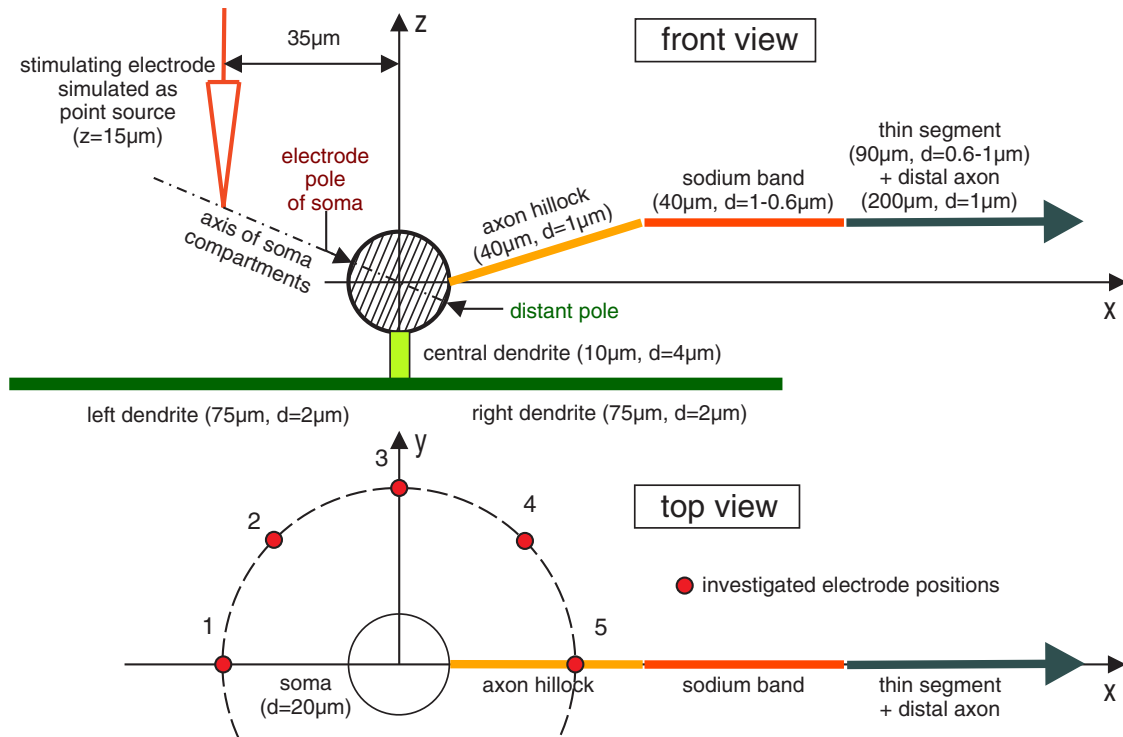


Figure 2. Geometry of the planar RGC model and investigated electrode positions. The compartment length of $1 \mu\text{m}$ is constant for all segments, except for the soma which consists of 21 compartments (length appr. $0.95 \mu\text{m}$) to model a compartment exactly at the center. While the compartments of the axon hillock, distal axon, and all dendritic parts are modeled as cylindrical structures, the segments of the spherical soma and the conical sections (sodium band, thin segment) are modelled as truncated cones.

Table 1. Simulated lower and upper thresholds in (μA) for monophasic cathodic and biphasic anodic-cathodic pulses for investigated electrode positions. The lower threshold is the lowest stimulus amplitude where an action potential was observed in the soma, which is at the same time the lower threshold for the whole RGC. At and above the upper threshold, no action potential was seen in the soma any more.

Pulse	Threshold	Pos. 1	Pos. 2	Pos. 3	Pos. 4	Pos. 5
Monophasic 0.25 ms	Lower threshold	4.7	4.4	4.4	3.2	0.5
	Upper threshold	21.3	20.6	20.9	19.8	1.6
Biphasic 0.25 ms	Lower threshold	4.7	4.7	4.8	3.7	0.6
	Upper threshold	27	27.3	29	25.4	16.2
Biphasic 0.5 ms	Lower threshold	3.1	3.1	3.2	2.4	0.4
	Upper threshold	20.4	19.5	20.4	18.3	14 ^a

^a As no clear border for the upper threshold can be determined in the simulation for the 0.5 ms biphasic case, the current indicates the rough border where the averaged membrane voltage of the soma surface will not exceed 0 mV at any time.

a representative cell in response to 0.25 ms pulse stimulation. Figure 3(B) illustrates raw traces from the same cell in response to 16 repetitions of 0.25 ms pulse stimulation with three different amplitudes: 50, 75 and 150 μA . There is no response to 50 μA stimulation, spikes to some pulses in response to 75 μA stimulation and spikes to all pulses in response to 150 μA stimulation. Subplots C and D in figure 3 show responses of the same cell to pulses of 0.375 ms duration. The blue curve in subplot C illustrates the upper threshold phenomenon, i.e. for stimulation amplitudes above 150 μA , the probability of eliciting a spike is decreased.

For the cell illustrated in figure 3, the upper threshold phenomenon was observed for longer pulse stimulation only. No upper threshold was observed for 0.25 ms pulse stimulation (no blue curve in figure 3(A)). The action potentials were observed for 0.25 ms duration and 150 μA amplitude stimulation (subplot B, right). However, for longer pulses (0.625 ms duration), the probability of spiking was decreased when a stimulation amplitude above 75 μA was applied (subplot C). There were no action potentials observed for 0.625 ms duration and 240 μA amplitude stimulation (subplot D, right).

An upper threshold phenomenon was also observed for all of our cells and pulse durations when the range of stimulation intensity was sufficiently large (blue curves in figure 4(A)). In four out of 21 cells, the upper threshold phenomenon was observed at only the longer pulse durations, most likely because the stimulator could not provide sufficient current amplitudes at the shorter durations, similar to data shown for the 0.25 ms pulse duration in figure 4(A). For one out of 21 recorded cells, the upper threshold phenomenon was never observed at any pulse duration or amplitude.

The decrease in activation probability beyond the peak value with increasing stimulus amplitude takes the shape of a negative sigmoid. Each star represents the probability of activation estimated over 16 presentations of a biphasic pulse, whose amplitude is shown on the x-axis and duration is shown at the top of the subfigures.

Figure 4(B) illustrates spike latency for the different phase durations, i.e. the time interval between stimulation onset and spike detection. A U-shaped pattern was observed for all phase durations except for 0.25 ms, for which the upper

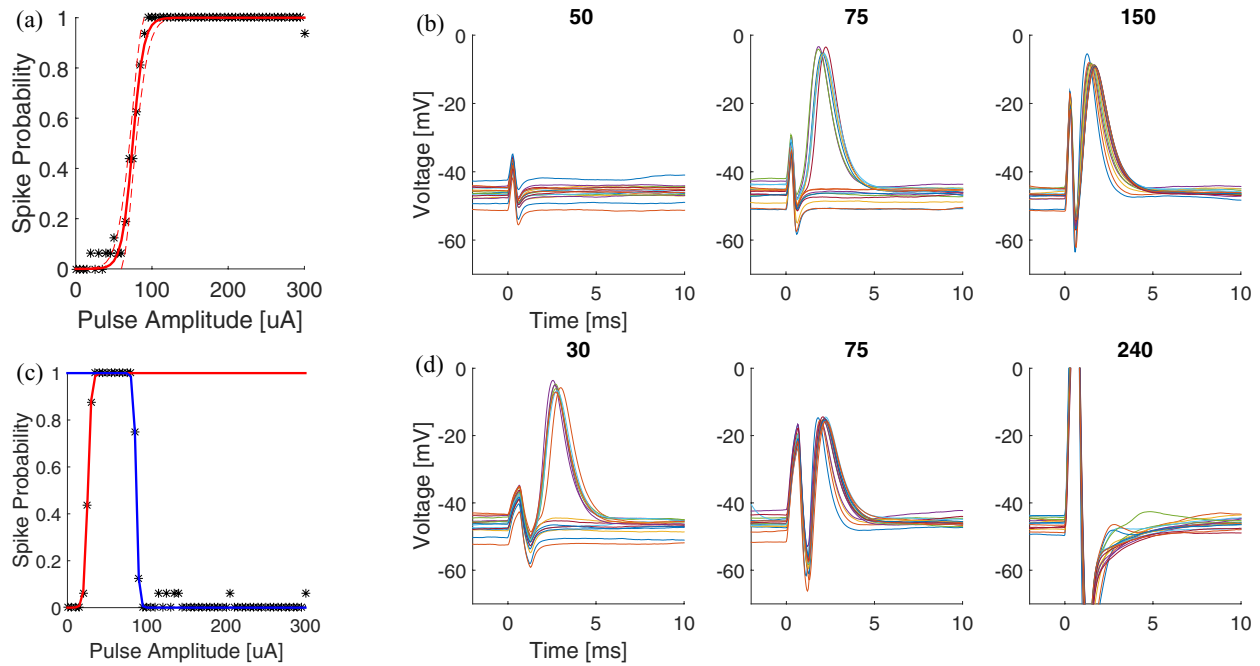


Figure 3. Response of an example cell to 0.25 ms (subplots (A) and (B)) and 0.625 ms (subplots (C) and (D)) pulse stimulation. ((A)–(C)) Sigmoid curve fit to data. ((B) and (D)) Raw traces in response to 16 repetitions of pulse stimulation. (B) 0.25 ms pulse with three amplitudes: 50, 75 and 150 μA . (D) 0.625 ms pulse with three amplitudes: 30, 75 and 240 μA . Dashed red lines in (A) illustrate the confidence interval corresponding to the 95% confidence level for the fitted parameters of the sigmoid.

threshold was not observed. This characteristic U-shape was previously reported by Boinagrov *et al* (2012). Figure 4(B) shows an example cell, counting only short latency (less than 4 ms) spikes.

In addition to the upper threshold phenomenon described above, another unexpected behavior was observed in 5 out of 21 of the patched cells. Sometimes, increasing stimulation amplitude far above the (initial) upper threshold led to a secondary increase in RGC activation. Figure 5(A) shows the activation curves for one representative cell that displayed this behavior. The number of spikes in response to stimulation amplitudes above the (initial) upper threshold level, increased in a linear fashion (the last four subfigures in A).

In these cells, it appears that low-amplitude stimulation induces short latency spikes (<4 ms), whereas high amplitude stimulation induces long latency spikes (≥ 4 ms). Indeed, both pools of spikes differ from each other in terms of latency, with low variability within each group. It is interesting to see that long latency spikes (figure 5(B)) can be clearly separated from short latency spikes. The mean value of the latencies of the long latency spikes varied across the population of cells. However, it remained consistent across pulse durations within individual cells.

In this work, the standard threshold of activation was defined as the pulse amplitude corresponding to the activation probability of 50%. Because there is both a positive sigmoid and a negative sigmoid fitted to the experimental data, there exist two thresholds of activation that are referred to as the lower threshold (associated with the positive sigmoid) and the upper threshold (associated with the negative sigmoid). In figure 6(A), red curves represent the lower thresholds found for individual cells for the different pulse durations,

while blue curves represent the upper threshold phenomena. Population data is shown for 16 out of 21 cells that showed the upper threshold phenomenon for all phase durations except 0.25 ms. Data for the upper threshold corresponding to the shortest pulse duration are missing. It is likely, that for these stimulation parameters the upper threshold value exceeded the stimulator's upper limit for some cells. This hypothesis is left to be examined.

The contour plot in figure 6(B) is another way of aggregating the data and provides a visual representation of the expected level of activation, given the combination of pulse amplitude and pulse duration. It consists of a two-dimensional space with pulse duration on its x -axis and pulse amplitude on its y -axis. Brighter colors (yellow) indicate higher activation probability and darker colors (red) correspond to lower activation probability.

3.2. Numerical simulations

To study the upper threshold phenomena in detail and explore its mechanisms, we simulated a model neuron in response to biphasic pulses of different amplitudes, durations, and electrode positions in the NEURON environment.

3.2.1. Monophasic pulse stimulation. Extracellular voltage, V_e , was calculated for a spherical electrode as $V_e = \rho_e I / 4\pi r$ (Rattay 1999), where r is the distance of the point of interest to the center of the electrode, ρ_e is the extracellular resistivity, and I is the stimulation current. The r -ratio for the closest point of the soma (the electrode pole, figure 2) to the distant pole of the soma is $48 \mu\text{m} / 28 \mu\text{m} = 1.71$. When stronger pulses are applied, the 71% higher extracellular potential at the electrode pole (relative to the distant pole) is the physical

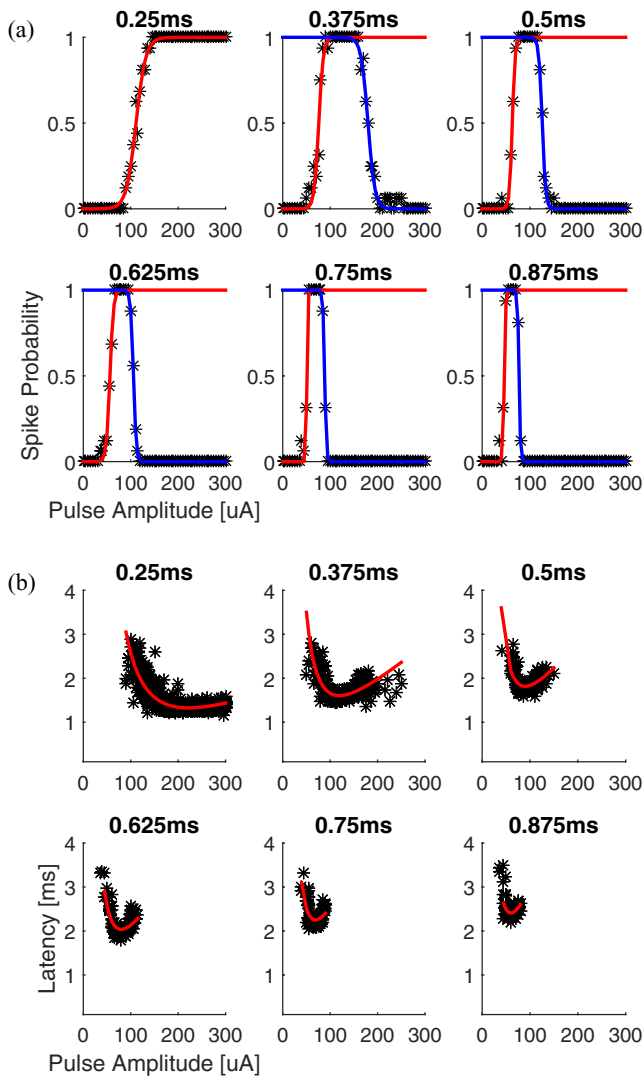


Figure 4. Activation of an example cell in response to biphasic pulses of different phase durations (indicated above each subplot). (A) The activation probability is plotted versus pulse amplitude for six different pulse durations. Stars represent experimental data. Red curves are the fitted positive sigmoids to the growing part of the data. Blue curves are the fitted negative sigmoids to the decreasing part. Each probability value is computed as an average over 16 repetitions of the stimulus. (B) Latency of spikes in the same cell as in (A). This type of analysis was repeated across all patched cells. Red curves are the fitted trendlines to short latency spikes data.

basis for sodium current reversal for cathodic stimulation. Note that the most sensitive part of the neuron is the axon (Rattay and Wenger 2010) and especially the sodium band (Jeng *et al* 2011, Werginz *et al* 2014). As the electrode position 1 is furthest from the sodium band (figure 2), this case is used in the following examples in order to concentrate on the lower and upper threshold phenomena occurring in the soma, where the experimental patch recordings were made.

Usually, electrical nerve stimulation aims to elicit an action potential by depolarizing the membrane voltage somewhere above a threshold value in order to open in this pre-excited region voltage sensitive sodium channels, which amplify the depolarizing effect with an inward sodium current. The left parts of figure 7 underline this principle: during cathodic

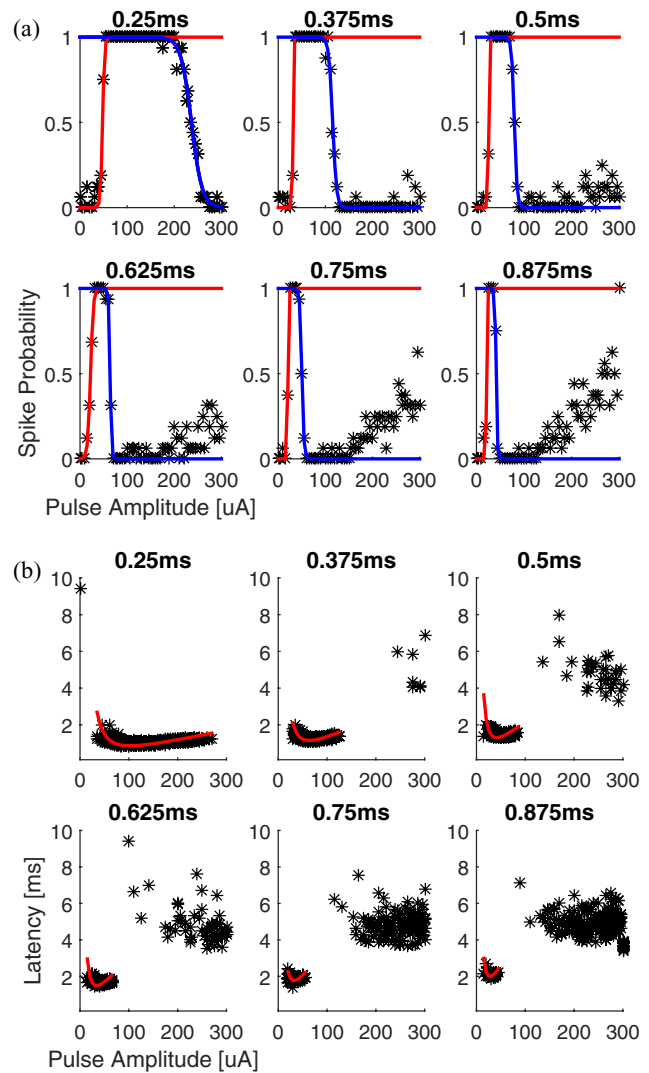


Figure 5. Activation of an example cell with long latency spikes in response to biphasic pulses of different phase durations (indicated above each subplot). (A) The activation probability is plotted versus pulse amplitude for six different pulse durations. Red curves are the fitted positive sigmoids to the growing part of the data. Blue curves are the fitted negative sigmoids to the decreasing part. Each probability value is computed as an average over 16 repetitions of the stimulus. (B) Latency of spikes in the same cell as in (A). An example cell with short and long latency spikes. Two distinct pools of spikes can be observed: short latency spikes elicited by lower pulse amplitudes and long-latency spikes elicited by higher pulse amplitudes. The difference between the mean latencies of these two clusters supports the hypothesis that long latency spikes are network mediated. Red curves are the fitted trendlines to short latency spikes data.

pulse application the averaged membrane voltage of the soma (black line in the left upper part) reaches threshold voltage and causes an action potential with a considerable delay. This delay decreases for stronger pulses as expected from theory and experiments made in different types of neurons (Rattay 1990). Further stimulus increase causes large membrane voltages at the electrode pole leading to outward sodium current as soon as sodium reversal potential (Nernst potential) is reached (figure 7, bottom right and insert, which causes the upper threshold phenomenon (Boinagrov *et al* 2012). Although there is no action potential

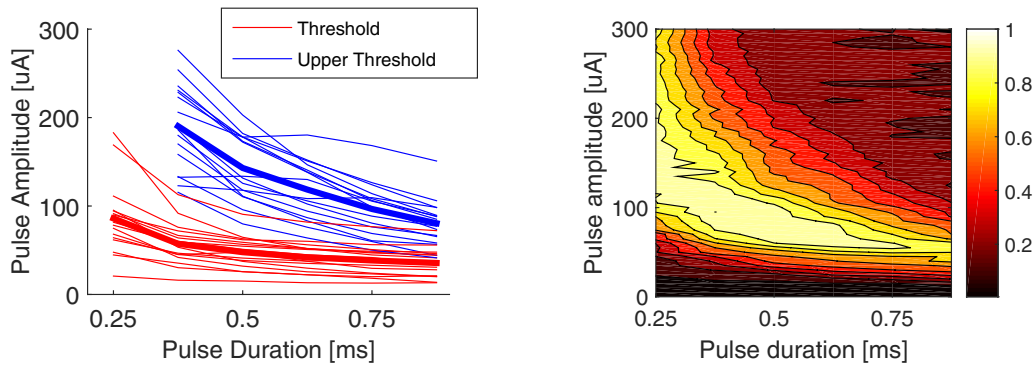


Figure 6. (A) Strength-duration relationship at the population level ($n = 16$). Average activation thresholds are plotted versus pulse duration. Red lines represent lower thresholds for individual cells (50% probability of activation for positive (red) sigmoids). Blue lines show 50% probability of activation for negative (blue) sigmoids. Thick lines indicate averages. (B) Contour plot of the strength-duration relationship at the population level ($n = 16$). Brighter colors represent areas of high activation probability, while darker colors correspond to low activation probability.

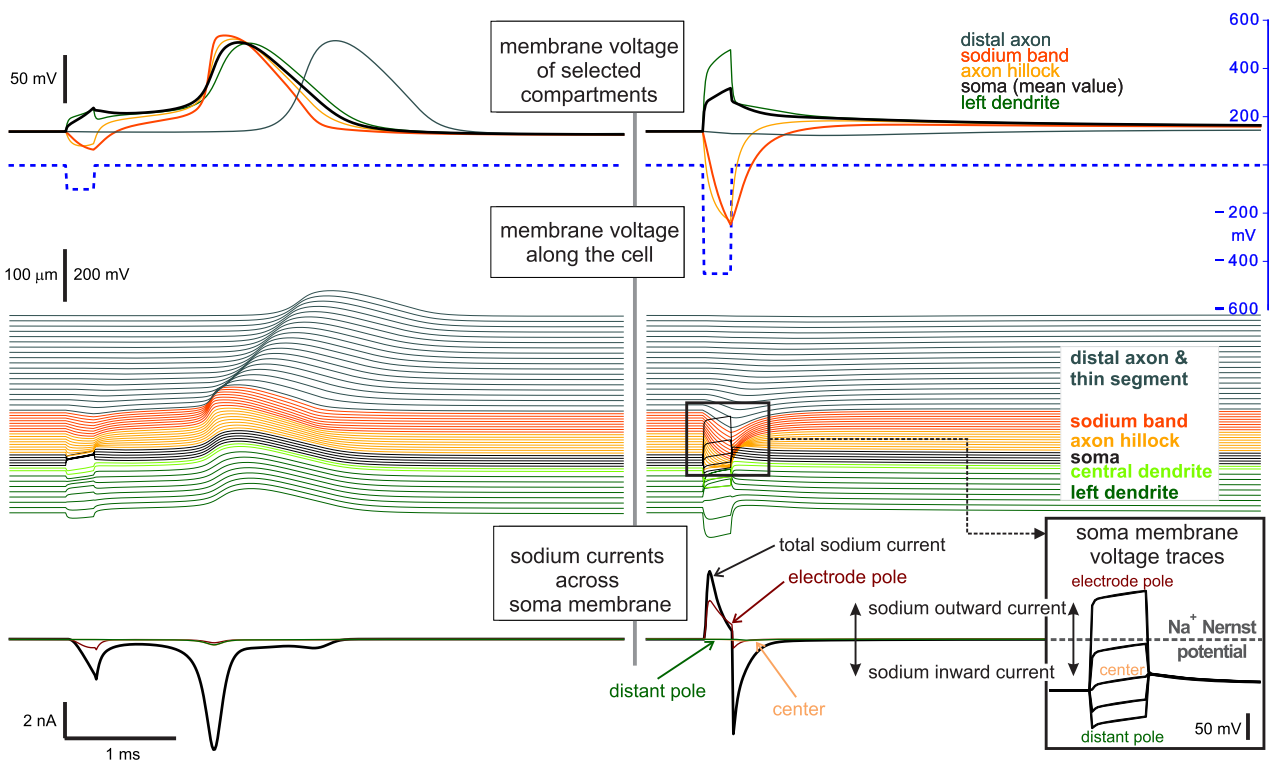


Figure 7. Transmembrane voltages and somatic sodium currents at lower threshold (left, $4.7 \mu\text{A}$) and upper threshold (right, $21.3 \mu\text{A}$) in response to monophasic cathodic 0.25 ms pulses (top, blue lines) for the electrode position 1. The central parts show the excitation of selected compartments with a vertical shift corresponding to the spatial extension of the cell. During pulse application, the membrane voltages along the soma surface differ essentially (black rectangle, center right), which are depicted as enlarged versions without vertical shifts in the insert (bottom right). During the pulse, the highest line of the insert, that is at the electrode pole, exceeds the sodium Nernst potential and causes outward sodium ion currents whereas the region around the distant pole is hyperpolarized without any sodium ion current. Scaling for the averaged extracellular potential is given by the blue axis labels (top, right).

seen in the right part of figure 7, rather large membrane voltages appear in the soma (black line, top) and in the left dendrite (green line, top) which cannot generate an action potential because of the hyperpolarized neighbored compartments, a phenomenon known as anodal surround block or cathodic block (Ranck 1975, Rattay 1990). This monopolar cathodic stimulation causes a total block of action potentials in the neuron.

The effect of the electrode positions 1–5 (refer to figure 2) on thresholds for different types of stimulation is given in

table 1. For cathodic monophasic 0.25 ms stimulation, at position 1–3 not only the soma but the whole cell is blocked at and above the upper threshold. For position 4 and 5, an action potential can also be observed in the axon above the upper threshold amplitude before the cell is finally completely blocked (Pos. 4: $-35.5 \mu\text{A}$, Pos.5: $-5.2 \mu\text{A}$). The rectangular monophasic cathodic pulse finally leads not only to a blocking of the soma but also to a blocking of the axon once a certain amplitude is exceeded. This was verified for all tested positions.

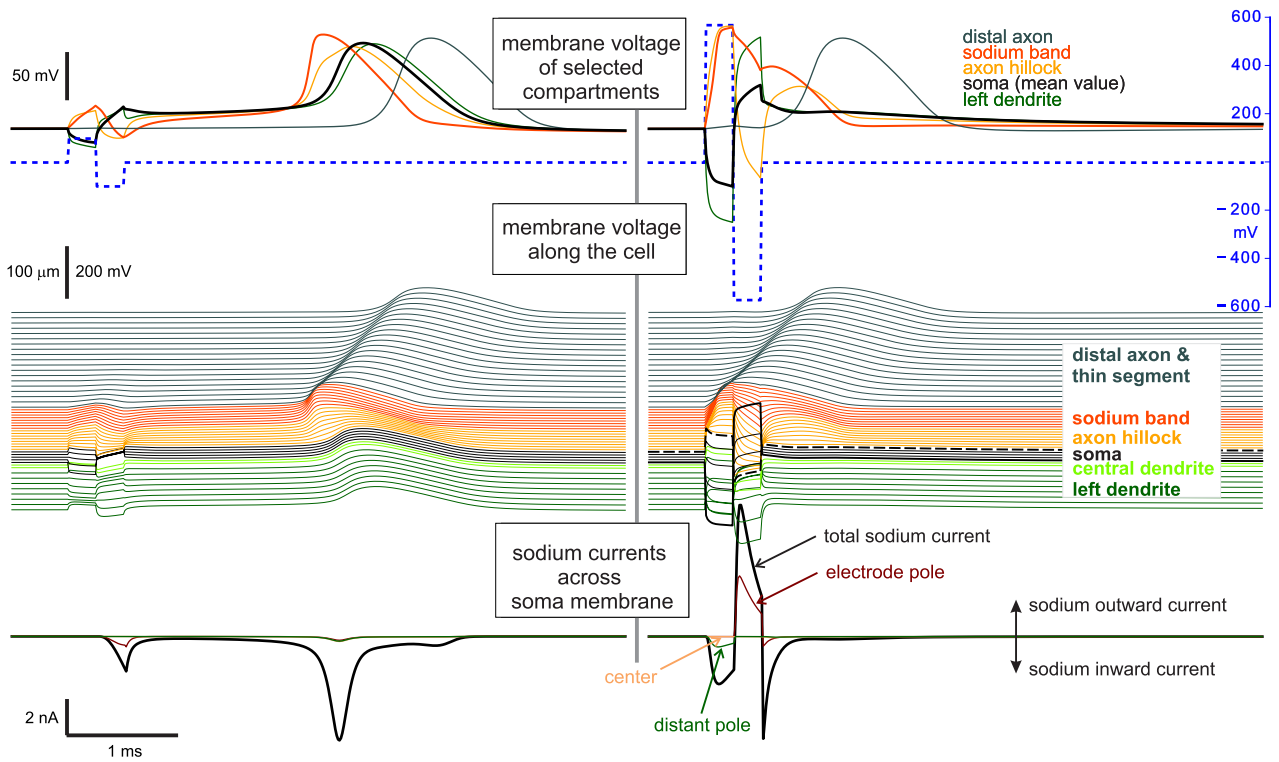


Figure 8. Transmembrane voltages and somatic sodium currents at lower threshold (left, 4.7 μA) and upper threshold (right, 27 μA) in response to biphasic pulse 0.25 ms phase duration, anodic first, for the electrode position 1. Same layout as in figure 7.

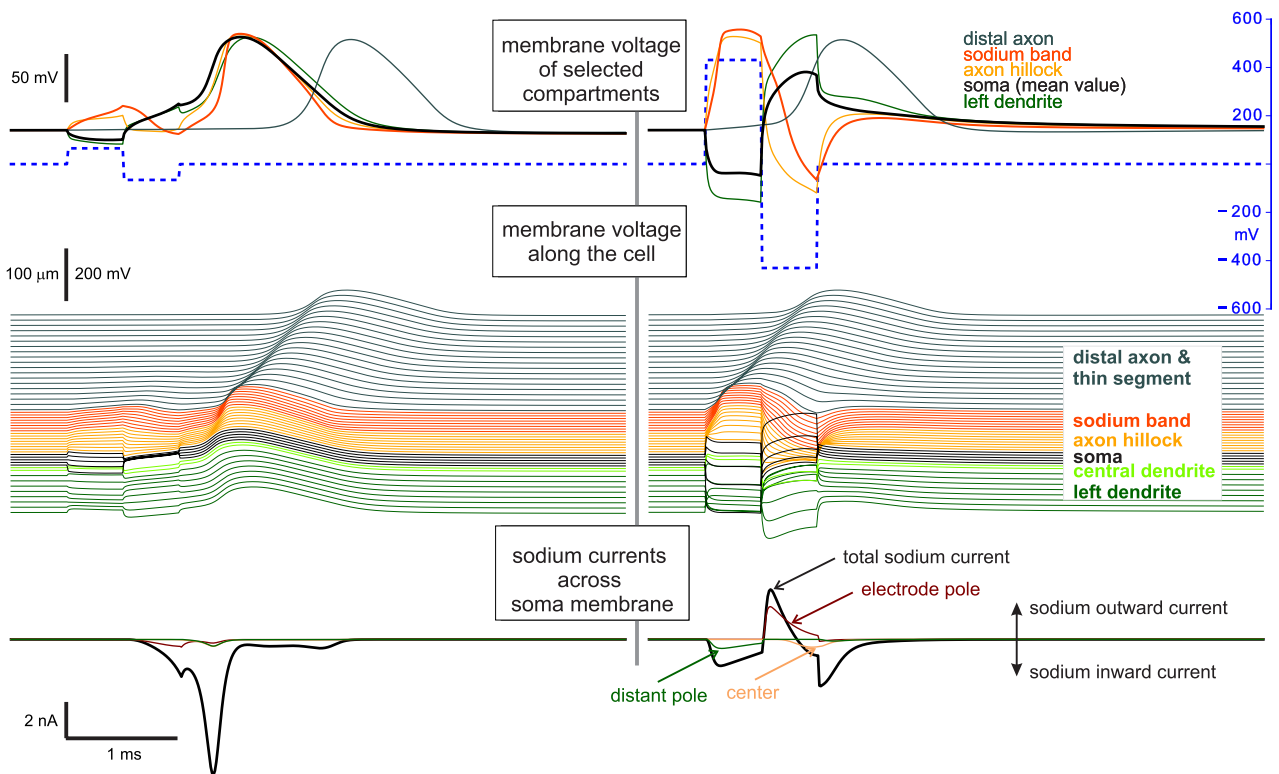


Figure 9. Transmembrane voltages and somatic sodium currents at lower threshold (left, 3.1 μA) and upper threshold (right, 20.4 μA) in response to biphasic 0.5 ms pulses, anodic first, for the electrode position 1. Same layout as in figure 7.

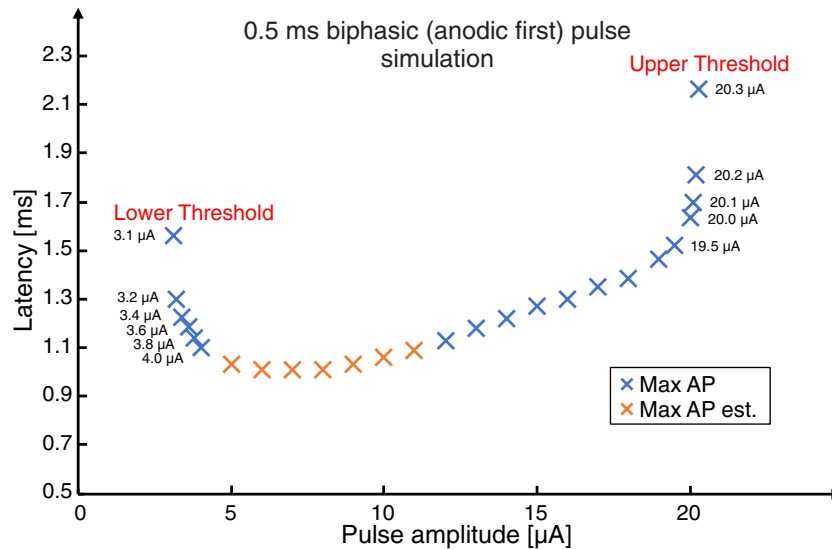


Figure 10. Simulated U-shaped latency pattern of somatic action potentials in response to biphasic anodic-first pulses, 0.5 ms phase duration, for the whole stimulation window (3.1–20.3 μA) for electrode position 1. The latency times marked blue were identified by the maximum peak of the average membrane voltage at the soma after the end of stimulus. The latency times marked orange were estimated by comparing the timing of respective soma membrane voltages among each other during the stimulus (because the membrane voltage peak and the stimulus times were overlapping).

3.2.2. Biphasic pulse stimulation. While the lower threshold for a biphasic pulse at 0.25 ms per phase was found to be at 4.7 μA , similar to monophasic stimulation, the positive pre-pulse results in a delayed action potential compared to the 0.25 ms monophasic case (compare figures 7 and 8, left). Note the weak depolarization during the first anodic phase in the axon hillock and sodium band (figure 8, top and center left), which causes a conducted action potential in the axon when the stimulus is increased (figure 8, center right). Opposite to the case of figure 7, the changed polarity of the first phase causes a strong hyperpolarization of the electrode pole region of the soma (figure 8, center right, thick black line) and a weak depolarization near the distant pole (figure 8, center right, broken black line) resulting in inward sodium ion currents (figure 8, bottom right). The phenomenological behavior does not change when longer biphasic pulses are applied (figure 9).

Simulated latency times for different stimulation amplitudes are illustrated in figure 10 for biphasic pulses with 0.5 ms duration. The stimulation leads to the U-shaped pattern of latencies of action potentials, similar to the experimental results of this study. Note the very strong increases in latency times on both ends of the stimulation window.

For investigated electrode positions 1–4, during the anodic phase the hyperpolarized regions in the soma dominate, while in the cathodic phase the depolarizing regions become dominant (compare thick black lines in figures 8 and 9, top and center). Therefore, an action potential in the soma can only appear during or after the depolarizing cathodic phase. The level of depolarization is crucial for any active cell membrane dynamics which are caused by voltage sensitive ion channels. When stimulus amplitudes are increased, the maximum voltage in the soma becomes gradually reduced during the second phase (figure 11) as a result of strong hyperpolarization originating from the first anodic phase of the biphasic stimulus and strong somatic sodium outward currents during

the second phase. Using high amplitudes, the averaged soma membrane voltage could always be forced below the resting voltage of -65 mV.

However, independent of the somatic upper threshold, even for much higher amplitudes (tested with 100 μA for all positions and pulse durations), a propagating action potential in the distal axon was observed in our simulations. Depending on the position of the electrode, those axonal action potentials were first initiated between the axon hillock (for the electrode position 1) and the end of the sodium band (for the electrode position 5) during the first anodic phase of the biphasic pulse. Note also the increase in action potential delay before the upper threshold level is reached (red lines in figure 11). This is in accordance with the experiments presented here and those of Boinagrov *et al* (2012).

Threshold amplitudes of lower and upper thresholds for the biphasic anodic first pulses are shown in table 1 for 0.25 and 0.5 ms pulses. For biphasic anodic first pulses, at the lower threshold the action potential is always initiated in the cathodic phase. Depending on the electrode position and amplitude, the first initiation might even occur in the soma itself. At higher amplitudes, the action potential is initiated already in the first anodic phase of the biphasic pulse. At and above the upper threshold the soma is blocked but, still, an action potential always propagated into the distal axon.

Moving the electrode to position 5 reduces the threshold for axonal spikes dramatically as a consequence of its short 6.8 μm distance to the axon hillock. As observed for all positions, near the lower threshold the action potential has a long latency time (see figure 10 for electrode position 1). The action potential slowly propagates back to the soma with a delay of approximately 1.2 ms. The reason for this long delay is found in the model geometry where the thin axon hillock is a bottleneck for back-propagating action potentials. Because of its small diameter, the intracellular resistance of the axon hillock is high while generated active cell membrane currents are low. This makes

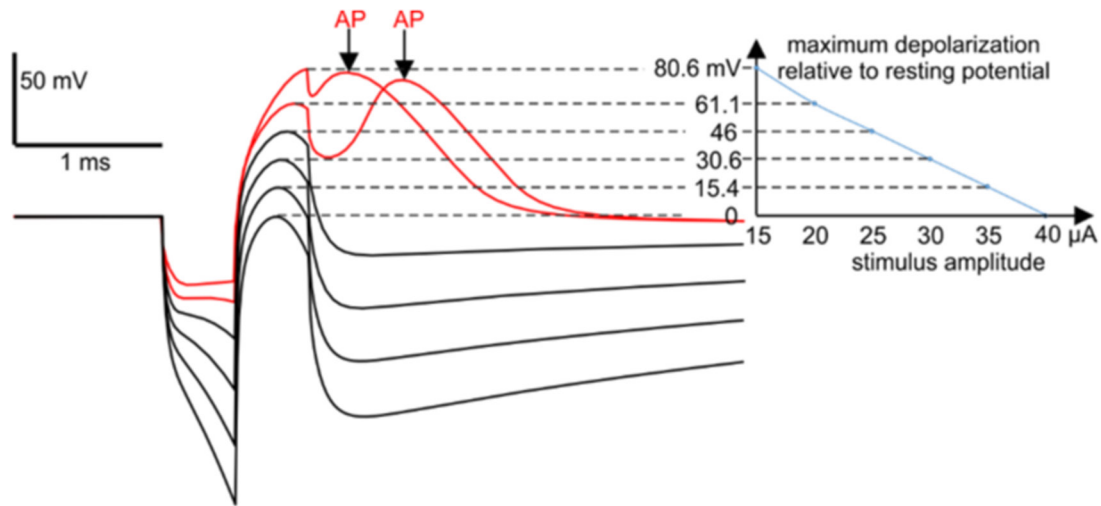


Figure 11. Action potential suppression in the soma and maximum depolarization depend on stimulus amplitude. Membrane voltages, averaged over all soma compartments, are shown for increasing pulse amplitudes from 15 to 40 μA . The simulation corresponds to figure 9 (0.5 ms biphasic pulse, electrode position 1) where upper threshold is 20.4 μA . Note the linear decrease of the maximum depolarization leading to a pure hyperpolarized response for amplitudes greater 40 μA . Holding potential for the first ms is -65 mV which is equal to the resting membrane potential.

it difficult for the axon hillock to provide enough intracellular current to depolarize the large soma. Additionally, at position 5 the hyperpolarized left and central dendrites during the cathodic phase slow down any depolarization of the soma.

However, because of the long latency time of the action potential at lower threshold amplitudes, there is enough time for the axon hillock to depolarize the soma slowly after the stimulus has ended so a somatic action potential is initialized. But at higher stimulus amplitudes, we found an additional range above the lower threshold where back-propagating action potentials cannot elicit a spike in the soma. At position 5, the soma is blocked between 2 and 4.6 μA for 0.25 ms pulses, between 1.1 and 2.3 μA for 0.5 ms pulses. Within that limit, the depolarizing influence of the stimulus on the soma itself is still very limited, while action potentials are already initialized in the proximal axon at a very early stage. This leads to a situation, where not enough time and strength is left for the back-propagating action potential to depolarize the soma once the countering effects of the stimulus stop dominating. Above the upper limit of this blocking range, the level of somatic depolarization itself is already high enough so the limited intracellular depolarizing currents from the axon hillock are sufficient to again trigger a somatic action potential. This additional somatic block within the actual stimulation window can be reduced or totally resolved by increasing the diameter of the axon hillock, decreasing dendrite diameters, or decreasing intracellular resistivity.

Furthermore, in contrast to the other positions, at position 5 the initiation of an action potential was also observed in the first anodic phase in the soma because of the additional depolarizing effects of the axon hillock during the anodic phase.

4. Discussion and conclusions

This study presents *in vitro* data recorded from rat RGCs in response to extracellular biphasic pulse stimulation of

various amplitudes and phase durations. Results show that there is an optimal range of stimulation that leads to 100% activation at the level of individual RGCs. Above this level, short latency responses are completely suppressed. We found that the optimal range of activation varied between RGCs. We found that the spike efficacy falls for high amplitudes of stimulation, displaying the upper threshold phenomenon for spikes recorded in the soma. All but one cell showed the upper threshold phenomenon for direct spikes recorded in the soma. For the cell that did not show decreases in spiking for high stimulation amplitudes, it is possible that the maximum amplitude limit was not sufficient to cause the upper threshold phenomenon.

Short and long latency spikes were classified based on the time interval between the stimulation artefact and the detected spike. Variability of spike latencies across the population, along with the consistency within each cell, supports the hypothesis that long latency spikes were due to retinal network activation. Long latency spikes have been shown to be network-mediated (Boinagrov *et al* 2014). We did not observe the upper threshold phenomenon for long latency spikes. No synaptic blockers were used in this study. To confirm that the upper threshold phenomenon occurs for direct but not indirect stimulation is left for future research.

The upper threshold phenomenon was observed *in vitro* by Barriga-Rivera *et al* (2017). While Boinagrov *et al* (2012) were not able to measure upper threshold for pulse durations above 0.5 ms due to strong interference between action potentials and artifacts, our work shows that it is possible to remove artifacts and observe upper threshold phenomena when the stimulation amplitude range is large enough. Variations were observed regarding various parameters, including the steepness of both sigmoidal curves, the values of the lower and upper thresholds of activation, and the length of the optimal range of stimulation (i.e. the amplitude range where the probability of a spike is one).

Experimentally, we recorded only the soma's response to stimulation—no axonal recordings were attempted. Numerical simulations showed that in all investigated cases above the lower threshold, a propagating action potential was recorded in the distal axon when using biphasic pulses. At amplitudes near the lower threshold, the position of the electrode determines if the action potential is initiated in the soma itself. However, for stronger amplitudes, axonal action potentials are always initiated in the sodium band or in the axon hillock. This was also confirmed for amplitudes far above the somatic upper threshold. In the investigated positions of the electrode, only strong monophasic cathodic pulses were able to cause total blocking of an action potential initiation.

The mono-phasic case is in accordance with Boinagrov *et al*'s (2012) observations concerning both amplitudes for lower and upper thresholds resulting in a ratio of the two parameters of $18.3/3.3 = 5.5$. This factor is larger for biphasic stimulation, more pronounced for the longer pulses, and larger compared to the experimental recordings.

All evaluated electrode positions have the same 28 μm distance to the soma surface. Consequently, the variations in lower and upper thresholds are small as long as the electrode is not close to the axon hillock (electrode positions 1–3, table 1). However, for position 5 the short axon hillock distance of 6.8 μm results in extremely low threshold values.

Further, for position 5 we observed additional blocks of the soma within the stimulation window (due to limited back-propagation capabilities of the thin axon hillock) and action potentials that were not time locked. In general, an electrode very near the sensitive proximal axon causes different effects near and in the soma, compared to other electrode positions. Nevertheless, an action potential does propagate to the distal axon in every case. The U-shaped delay of action potentials as a function of stimulus intensity is seen both for mono- and biphasic pulses. In this work, we did not test for the effect of asymmetric biphasic pulses on the upper stimulation threshold. This is left for future work.

We found variability in the optimal range of stimulation amplitudes for individual cells. This variability may be due to the cell specific intrinsic electrophysiology and morphology, or difference in electrode placement, which was not vigorously controlled (Wong *et al* 2012). These results may have implications for stimulation strategies in retinal implants targeted to preferentially activate individual cell types. To this extent, Hadjinicolaou *et al* (2015) proposed an optimized waveform to improve the efficacy of electrical stimulation of RGCs. Previous studies characterized the strength-duration relationship in RGCs (Jensen *et al* 2005, Sekirnjak *et al* 2006, Tsai *et al* 2009). This relationship is nonlinear, such that the activation threshold found for short pulses may be extremely high.

It has been shown that the response probabilities of RGCs decrease over time for repetitive pulse stimulation. The decrease in spiking probability is more pronounced when there are short intervals between pulses, i.e. higher stimulation frequencies (Jensen and Rizzo 2007). Jensen and Rizzo (2007) observed decreases in spike probability for stimulation frequencies as

low as 10 Hz. We did not investigate this phenomenon in this study. Our choice of 20 Hz stimulation was based on the ability to detect short and long latency spikes between pulses (within a 50 ms window) and to avoid the dependency of consecutive pulse stimulation on the responses. Some other studies demonstrated that certain RGC types could reliably follow pulse rates up to 600 Hz Cai *et al* (2011). At the clinical level, Nanduri *et al* (2012) characterized how pulse frequency and amplitude modulation affect perception. In particular, it was found that increasing frequency always increases pixel brightness, while increasing amplitude increases both pixel size and brightness. As a general conclusion, Nanduri *et al* (2012) suggested that only stimulation frequency should be modulated to encode brightness levels to avoid losing spatial resolution.

Electrical stimulation of neural tissue is the basis of neural prostheses and treatments for many neurological disorders (Cogan 2008). Most studies in the field of neuroprosthetics do not report the upper threshold phenomenon and assume saturation of the activation curve. Our numerical simulations show that even if the soma is blocked, the action potential is still initiated in the proximal axon and propagated to the distal axon when using biphasic anodic first pulses. However, this is yet to be confirmed experimentally.

In some cases of monophasic cathodic stimulation the upper threshold in the soma hinders axonal excitation (figure 7), whereas other electrode positions cause one-sided axonal firing (Rattay 2014). Some evidence for axonal firing during somatic block comes from the *in vivo* experiments by Barriga-Rivera *et al* (2017), where high amplitude stimuli did not reduce axonal firing recorded in the visual cortex, which was opposite to their expectations from *in vitro* recording.

We found that an upper threshold observed in the soma does not prevent spike conduction in the axon. Therefore, results obtained using an *in vitro* setup, with recording in the soma, should be carefully considered when making assumptions about the spike conduction sent into the brain. This may have important implications for the development of stimulation strategies in visual prostheses.

Acknowledgments

This research was partly supported by the Australian Research Council through the Centre of Excellence for Integrative Brain Function (CE140100007). TK acknowledges support through the Australian Research Council Discovery Projects funding scheme (DP140104533). This work was supported by the Austrian Science Fund (FWF), grant no. 29650.

ORCID iDs

Andreas Fellner  <https://orcid.org/0000-0003-3704-8764>
 Frank Rattay  <https://orcid.org/0000-0002-2819-8827>
 Diego Ghezzi  <https://orcid.org/0000-0002-0554-7510>
 Hamish Meffin  <https://orcid.org/0000-0003-4307-6841>
 Michael R Ibbotson  <https://orcid.org/0000-0002-3803-6653>
 Tatiana Kameneva  <https://orcid.org/0000-0003-0081-8569>

References

- Barriga-Rivera A, Guo T, Yang C-Y, Abed A A, Dokos S, Lovell N H, Morley J W and Suaning G J 2017 High amplitude electrical stimulation can reduce elicited neuronal activity in visual prosthesis *Nat. Sci. Rep.* **7** 42682
- Boinagrov D, Pangratz-Fuehrer S, Suh B, Mathieson K, Naik N and Palanker D 2012 Upper threshold of extracellular neural stimulation *J. Neurophys.* **108** 3233–8
- Boinagrov D, Pangratz-Fuehrer S, Goetz G and Palanker D 2014 Selectivity of direct and network-mediated stimulation of the retinal ganglion cells with Epi-, Sub- and Intra-Retinal electrodes *J. Neural Eng.* **11** 026008
- Cai C, Ren Q, Desai N J, Rizzo J F and Fried S I 2011 Response variability to high rates of electric stimulation in retinal ganglion cells *J. Neurophys.* **106** 153–62
- Cogan S F 2008 Neural stimulation and recording electrodes *Annu. Rev. Biomed. Eng.* **10** 275–309
- Fohlmeister J F, Cohen E D and Newman E A 2010 Mechanisms and distribution of ion channels in retinal ganglion cells: using temperature as an independent variable *J. Neurophys.* **103** 1357–74
- Fohlmeister J F and Miller R F 1997 Impulse encoding mechanisms of ganglion cells in the tiger salamander retina *J. Neurophys.* **78** 1935–47
- Freeman D K, Rizzo J F III and Fried S I 2011 Encoding visual information in retinal ganglion cells with prosthetic stimulation *J. Neural Eng.* **8** 035005
- Hadjinicolaou A E, Meffin H, Maturana M I, Cloherty S L and Ibbotson M R 2015 Prosthetic vision: devices, patient outcomes and retinal research *Clin. Exp. Optom.* **98** 395–410
- Hamel C 2006 Retinitis pigmentosa *Orphanet J. Rare Diseases* **1** 40
- Hamill O P, Marty A, Neher E, Sakmann B and Sigworth F J 1981 Improved patch-clamp techniques for high-resolution current recording from cells and cell-free membrane patches *Pflügers Archiv.* **391** 85–100
- Hines M 1993 NEURON a program for simulation of nerve equations *Neural Systems: Analysis and Modeling* ed F Eckman (Norwell, MA: Kluwer)
- Jeng J, Tang S, Molnar A, Desai N J and Fried S I 2011 The sodium channel band shapes the response to electric stimulation in retinal ganglion cells *J. Neural Eng.* **8** 036022
- Jensen R J, Ziv O R and Rizzo J F 2005 Responses of rabbit retinal ganglion cells to electrical stimulation with an epiretinal electrode *J. Neural Eng.* **2** S16
- Jensen R J and Rizzo J F III 2007 Responses of ganglion cells to repetitive electrical stimulation of the retina *J. Neural Eng.* **4** S1
- Maturana M I, Apollo N V, Hadjinicolaou A E, Garrett D J, Cloherty S L, Kameneva T, Grayden D B, Ibbotson M R and Meffin H 2016 A simple and accurate model to predict responses to multi-electrode stimulation in the retina *PLoS Comput. Biol.* **12** e1004849
- Meffin H, Tahayori B, Grayden D B and Burkitt A N 2012 Modeling extracellular electrical stimulation: I. Derivation and interpretation of neurite equations *J. Neural Eng.* **9** 065005
- Nanduri D, Fine I, Horsager A, Boynton G M, Humayun M S, Greenberg R J and Weiland J D 2012 Frequency and amplitude modulation have different effects on the percepts elicited by retinal stimulation *Investigative Ophthalmol. Vis. Sci.* **53** 205–14
- Ranck J B 1975 Which elements are excited in electrical stimulation of mammalian central nervous system: a review *Brain Res.* **98** 417–40
- Rattay F 1990 *Electrical Nerve Stimulation* (Wien: Springer)
- Rattay F 1999 The basic mechanism for the electrical stimulation of the nervous system *Neuroscience* **89** 335–46
- Rattay F 2014 On the upper threshold phenomenon of extracellular neural stimulation *J. Neurophysiol.* **112** 2664–5
- Rattay F and Wenger C 2010 Which elements of the mammalian central nervous system are excited by low current stimulation with microelectrodes? *Neuroscience* **170** 399–407
- Sekirnjak C, Hottowy P, Sher A, Dabrowski W, Litke A M and Chichilnisky E J 2006 Electrical stimulation of mammalian retinal ganglion cells with multielectrode arrays *J. Neurophysiol.* **95** 3311–27
- Tsai D, Morley J W, Suaning G J and Lovell N H 2009 Direct activation and temporal response properties of rabbit retinal ganglion cells following subretinal stimulation *J. Neurophysiol.* **102** 2982–93
- Tsai D, Chen S, Protti D A, Morley J W, Suaning G J and Lovell N H 2012 Responses of retinal ganglion cells to extracellular electrical stimulation, from single cell to population: model-based analysis *PLoS One* **7** e53357
- Weiland J D and Humayun M S 2014 Retinal prosthesis *IEEE Trans. Biomed. Eng.* **61** 1412–24
- Wong R C S, Cloherty S L, Ibbotson M R and O'Brien B J 2012 Intrinsic physiological properties of rat retinal ganglion cells with a comparative analysis *J. Neurophysiol.* **108** 2008–23
- Wong W L, Su X, Li X, Cheung M G C, Klein R, Cheng C Y and Wong T Y 2014 Global prevalence of age-related macular degeneration and disease burden projection for 2020 and 2040: a systematic review and meta-analysis *Lancet Glob. Health* **2** e106–16
- Werginz P, Fried S I and Rattay F 2014 Influence of the sodium channel band on retinal ganglion cell excitation during electric stimulation—a modeling study *Neuroscience* **266** 162–77
- Yue L, Weiland J D, Roska B and Humayun M S 2016 Retinal stimulation strategies to restore vision: fundamentals and systems *Prog. Retinal Eye Res.* **53** 21–47